1-1995

A Comprehensive, Automated Approach to Determining Sea Ice Thickness from SAR Data

Donna Haverkamp
University of Kansas

Leen-Kiat Soh
University of Nebraska, lsoh2@unl.edu

Costas Tsatsoulis
University of Kansas, tsatsoul@eecs.ukans.edu

A Comprehensive, Automated Approach to Determining Sea Ice Thickness from SAR Data

Donna Haverkamp, *Student Member, IEEE*, Leen Kiat Soh, *Student Member, IEEE*, and Costas Tsatsoulis, *Member, IEEE*

***Abstract*—This paper documents an approach to sea ice classification through a combination of methods, both algorithmic and heuristic. The resulting system is a comprehensive technique, which uses dynamic local thresholding as a classification basis and then supplements that initial classification using heuristic geophysical knowledge organized in expert systems. The dynamic local thresholding method allows separation of the ice into thickness classes based on local intensity distributions. Because it utilizes the data within each image, it can adapt to varying ice thickness intensities to regional and seasonal charges and is not subject to limitations caused by using predefined parameters.**

I. Introduction

We developed a technique to determine sea ice thickness from Synthetic Aperture Radar (SAR) data. We implemented a dynamic local thresholding method to divide an image into separate ice thickness classes and coded human geophysical knowledge into expert systems in order to further substantiate or negate the initial classifications given by the dynamic local thresholding method.

Overview

Thresholding is a widely-used tool in sea ice classification. However, global thresholding is not always optimal for certain areas of an image. Small local changes which can be detected in a local histogram often disappear when surveyed in the context of a global histogram. If this global histogram is used to determine the intensity boundaries among the ice thickness classes, then the small local change is lost. Also, many global thresholding methods are not appropriate for determining ice thickness in areas where an excessive amount of melting and refreezing is taking place because of rapidly changing ice signatures. The technique for local thresholding that we developed can distinguish gray-level changes in small areas and is appropriate for preserving the visual contrast of the original image. It determines threshold points based upon the relative gray level intensities within the image and adapts easily to variation in the signatures of the ice thickness classes.

Classification based upon mere intensity is, however, limited by our own understanding of SAR and by the overlapping of the intensity groupings of different ice thicknesses. Humans are capable of using additional information to positively determine the classification of a given ice floe or formation of ice, such as qualitative models of sea ice growth and behavior in addition to historical and geographical information. Because of this, it was decided that geophysical knowledge could be used to improve initial classifications based upon local thresholding techniques.

To apply geophysical knowledge, the image is transformed into a higher level of representation, or a *feature* level. Every feature in the image is uniquely defined, and its identifying characteristics are obtained. Given this higher-level representation, human knowledge is applied in the form of expert system rules which embody geophysical information, along with the historical and geographical information necessary for an appropriate classification.

Our results show that this approach is appropriate for the classification of sea ice into its significant ice thickness categories. The dynamic local thresholding technique preserves the local contrasts in the image and achieves good separation among the ice thickness classes, while the expert systems help to avoid many misclassifications which commonly occur in classification techniques based purely on intensity.

1) Algorithmic Classification: Local Thresholding: The respective signatures of the different sea ice thickness classes vary throughout the year and over different regions of the polar oceans. Because of this inherent instability in the sea ice signatures, local thresholding was selected to produce the initial classification. Local thresholding selects threshold points based upon varying image intensities and the relative intensities within the images. As a result, it naturally follows and adapts to varying ice signatures as no global thresholding method possibly can. Our local thresholding technique separates the image into three distinct classes or ice thicknesses based upon gray level intensity.

2) High Level Image Translation: Feature Extraction: A separation of classes does not always ensure a separation of all the *features* within the image. For example, two ice floes which touch may appear as one single, strangely-shaped blob feature in the image. Leads are often discontinuous and broken into pieces. For the expert systems to properly analyze the features, each feature must be uniquely defined-features which are "touching" must be defined individually so that the expert systems have valid features with which to work. Given these extracted features, identifying characteristics can be obtained and associated with each feature. These characteristics consist of geometrical measures and of positional relationships among features in the image, which are used by the expert systems to assist in the analysis of the data.

Manuscript received December 2, 1993. This work was supported in part by a NASA Graduate Student Fellowship in Global Change Research (NGT-30189), and by NASA under Grant NAGW-3043.

The authors are with the Center for Excellence in Computer Aided Systems Engineering, Department of Electrical Engineering and Computer Science, The University of Kansas, Lawrence, KS 66045-2228 USA.

IEEE Log Number 9407080.

Digital Object Identifier: 10.1109/36.368223

3) Geophysical Knowledge Application: Expert Systems: The expert systems contain knowledge vital to the classification of sea ice. Utilizing knowledge concerning the geophysical processes at work in the ice, a better classification can be realized. The expert system rules embody qualitative, heuristic, expert models of sea ice growth and overall behavior. These rules also use knowledge concerning what ice thickness classes are likely to be found where during what time of the year, and what ice thickness classes *cannot* be found in certain areas at certain times of the year. Using this information, the feature level information can be analyzed accordingly and subsequent improvements in the initial classification can be achieved.

4) Expert Systems: Functional Viewpoint: Expert systems are being used in an ever-widening variety of applications in science, engineering, and business. Because of the simplicity involved in updating and/or changing its rules and the reasoning power of which it is capable, we believe that the expert system is an optimal choice as part of a system which is to use symbolic, expert knowledge and which is to be constantly updated to reflect new knowledge and new technology.

By applying knowledge to known facts, a human can use thought processes to generate new hypotheses, or facts (example: *facts*—it is raining, I am going outside; *knowledge*—if it is raining and I am going outside, then I should carry an umbrella; *new fact generated*—I will carry an umbrella). An expert system works in a parallel manner. Using a knowledge base and a fact base, it uses an *inference engine* to apply the knowledge to the facts and, thereby, generate new facts.

Facts represent the current state of the world—they tell the expert system *what things are true now*. As facts are added and deleted to and from the fact base, the state of the world changes. These changes may cause other rules in the knowledge base to fire and lead to further changes in the state of the world. The expert system stops when the state of the world has reached a steady state; that is, when no more rules will fire on the existing facts. When no more knowledge can be applied, no new facts can be generated; all that can be concluded about the state of the world has been deduced.

The reclassifications performed during the expert system stage are mapped back to the original classification image to show the final classification results. The resultant system fuses algorithmic methods and geophysical and historical knowledge to achieve a more accurate classification.

II. Related Work

A good deal of research has been performed in automatic classification of sea ice imagery. The oldest technique used is thresholding, which quantizes the image into discrete intensity levels. Some enhancements, implemented in [1]–[5], concerned manipulations of the data in order to clarify or sharpen the peaks of the histogram such that thresholds could be more accurately selected. These enhancements met with some success, but resulted in manipulations of the data itself, or biasing, to achieve class separations.

The JPL algorithm combines a clustering technique with a thresholding technique to classify data for the Alaska SAR Facility [6]. After clustering using the ISODATA algorithm, the clusters are compared to a look-up table consisting of backscatter values related to ice types. The brightest or highest-valued class is compared to the multi year ice value in the table, and then all of the other clusters are compared and defined. Every pixel in each cluster is then given the classification of that cluster as obtained from the look-up table.

Rule-based systems have been used in the past both for image segmentation on a pixel basis and for image analysis after image segmentation has been performed. One unique approach used expert systems to analyze an image in terms of characteristics concerning image quality and to then recommend the best algorithmic method to use for classification [7]. A related approach used expert systems to determine and then apply a set of algorithms for pre-classification image processing [8]. This procedure, however, also performed post-segmentation analysis of the image using a blackboard consisting of object-detection subsystems to identify all objects in the image. In [9], production rules were used to merge and split regions and to add, delete, and join lines in an image to pick out the separate features.

Multispectral remotely sensed data was the input of an expert system that made classification decisions on the pixel level [10]. The spectral rules contain information about characteristic spectral relationships, and were applied in a pyramid fashion, or in a way which worked on multiple resolution levels of the image. The rules were applied to reinforce or refute classification decisions by a multispectral classifier. Different expert systems were applied to different parts of the image and for different classification tasks. A *uniform expert* was used to verify that a pixel belonged to a large, uniform region, while a *border expert* was used to verify the classification of a pixel at the border of two regions, and a *noise expert* was used to verify that an abnormal pixel inside a uniform region was the result of noise.

An expert system to classify SAR imagery was presented in [11]. The system used approximately 100 rules to classify ice floes into different "age" categories. The user had to look at the SAR image and then input high-level information about each floe that had to be classified (for example, "there is a ridge" or "the flow shape is round," etc.). Other examples of the use of expert systems to classify SAR imagery may be found in [12].

III. Local Dynamic Thresholding

The signatures of ice thickness classes vary over the different polar regions, and they vary within those regions as the seasons change. No global thresholding method can compensate for all of those variations.

We adapted the local thresholding method of [13] to subdivide the image into three classifications. The image is first subdivided into many smaller regions; these regions are considered small enough to be at most bimodal (containing two types or thicknesses of ice). Criteria are applied to select those regions whose histograms are substantially bimodal. These

histograms are then used to calculate a single threshold using the Maximum Likelihood method. The calculated thresholds are clustered into two groups-one to represent the division between Class 1 and Class 2, the other to represent the division between Class 2 and Class 3. We then interpolate from regions with thresholds to other regions in the image to ensure that each region has two thresholds. A final interpolation is performed from the region down to the pixel level to provide each pixel with two threshold values. Finally, the actual thresholding is performed upon every pixel in the image, using the two threshold values determined for each pixel. Pixels are separated into one of three classes; these three classes represent ice thicknesses of 0–30 cm (traditionally called "open water/young ice"), 30–200 cm (traditionally called "first-year ice"), and >200 cm (traditionally called "multi year ice"), respectively.

Using this procedure, an image thresholding can be achieved which preserves local distinctions in the image, thus producing a more accurate quantized representation of the original image when compared visually to a global thresholding method.

A. Step 1: Division into Regions and Histogram Computation

The regions are selected by first defining the desired size of each region. Given this and the size of the image, the number of rows of regions in the image and the number of columns of regions in the image can be defined such that the overlap between any region and one of its 4-neighborhood neighbors is 50%. The intensity distribution, or histogram, of every region is computed individually and stored in a global histogram matrix.

B. Step 2: Selection of Regions of Large Variance

The variance of every histogram is computed through the equation:

$$\sigma_x^2 = E[x^2] - \{E[x]\}^2 = E[x^2] - \mu^2$$

which, expressed in terms of the histogram of each region, h, is:

$$\sigma_R^2 = \frac{\sum_{i=0}^{255} \left(\left(\frac{i}{255}\right)^2 * h[i]\right)}{\text{number of points in region}} - \left(\frac{\sum_{i=0}^{255} \left(\frac{i}{255} * h[i]\right)}{\text{number of points in region}}\right)^2.$$

The variable i is evaluated from 0 to 255 since these are the possible histogram bins.

By looking at the histograms created by regions and their corresponding variances, it was decided that it was necessary to change the variance threshold V_t for different types of images in order to be sufficiently accurate in identifying which histograms were possibly bimodal enough to have a Gaussian curve approximation performed. We set the variance threshold V_t to a value which allows *at least* 25% of the histograms to pass the variance test, ideally providing us with a sufficient number of regions from which to obtain thresholds.

C. Step 3: Gaussian Curve Approximation

This step is only performed for those regions whose variance, calculated in the previous step, is greater than some threshold V_t. From the publication of [14] and additional assistance from [15], the curve approximation was achieved.

1) Initial Parameter Estimation: To obtain good results from the curve-fitting algorithm, it was required to have good initial values for the parameters μ_1, μ_2, σ_1, and σ_2. To estimate μ_1, the mean of the histogram in the range [0, mean) was calculated, while the histogram mean in the range [mean, 255] was used to estimate μ_2. The corresponding standard deviations were calculated over those same ranges. Also calculated were initial values for the coefficients of mixture (see below), c_1 and c_2. These were calculated as the number of points represented in the range [0, mean) and the number of points represented in the range [mean, 255], respectively, divided by the total number of points in the region.

2) Gaussian Curve Approximation: The procedure used for finding a mixture of two Gaussians, which corresponds to the histogram data was taken from the method of [14].

The goal of the curve fitting is to approximate the probability function of the data, $f(x)$, by a set of $n(n = 2$, in this case) normal density functions:

$$\hat{f}(x) = \sum_{k=1}^{n} c_k \phi(x; \mu_k, \sigma_k)$$

where

$$\phi(x; \mu_k, \sigma_k) = \frac{1}{\sqrt{2\pi}\sigma_k} \exp\left[\frac{-(x-\mu_k)^2}{2\sigma_k^2}\right]$$

is the normal density function with mean μ_k and variance σ_k^2. The set of coefficients $\{c_k\}$ satisfy the constraints:

$$c_k \geq 0, \quad \sum_{k=1}^{n} c_k = 1.$$

Under these constraints, the estimate $\hat{f}(x)$ is a probability density function: $\hat{f}(x) \geq 0$ for all x, and $\int \hat{f}(x)dx = 1$.

To estimate from the samples $x_1, x_2, \cdots, x_n$ with the density function $f(x)$ the values of c_k, μ_k, and σ_k requires the maximization of the regression function

$$L \equiv \int f(x) \ln\{\hat{f}(x)\} dx = E_x\left[\ln\{\hat{f}(x)\}\right]$$

where $E_x[\bullet]$ indicates the expectation over the distribution of x. This function is the expected value of the log-likelihood function. Maximizing L is equivalent to minimizing the following error criterion

$$J \equiv \int f(x) \ln\left[\frac{f(x)}{\hat{f}(x)}\right] dx = E_x\left[\ln\frac{f(x)}{\hat{f}(x)}\right]$$

since $J \geq 0$ with equality if and only if $f(x) = \hat{f}(x)$ for almost all x.

To minimize J, the equation

$$L = E[\ln \hat{f}(x)]$$

must be maximized. The maximum occurs when the partial derivatives of L are zero. We solve for these partial derivatives iteratively. At the $(i+1)$th stage of estimation

$$\mu_k(i+1) = \mu_k(i) + \rho(i)\frac{\partial}{\partial \mu_k}\ln \hat{f}(i)\bigg|_{x=x_i}$$

$$\omega_k(i+1) = \omega_k(i) + \rho(i)\left[\frac{\partial \tau_k(i)}{\partial \omega_k}\frac{\partial}{\partial \tau_k}\ln \hat{f}(i)\right]\bigg|_{x=x_i}$$

$$\delta_k(i+1) = \delta_k(i) + \rho(i)\left[\sum_{l=k}^{n-1}\frac{\partial c_l(i)}{\partial \delta_k}\frac{\partial}{\partial c_1}\ln \hat{f}(i)\right]\bigg|_{x=x_i}$$

where

$$\omega_k = \tau_k - \frac{1}{\tau_k} = \frac{1}{\sigma_k} - \sigma_k \qquad 0 < \tau_k < \infty$$

$$\tau_k = \frac{1}{\sigma_k} = \frac{1}{2}\left(\omega_k + \sqrt{\omega_k^2 + 4}\right)$$

$$\delta_k = \frac{2c_k - (1-d_k)}{c_k(1-d_k-c_k)} \qquad 0 \le c_k \le 1 - d_k$$

$$c_k = \frac{1}{2\delta_k}\left[(1-d_k)\delta_k - 2 + \sqrt{(1-d_k)^2\delta_k^2 + 4}\right]$$

and where x_i is the ith observation (i.e., a value picked from the histogram or the region), and $\rho(i)$ is a sequence of positive numbers satisfying

$$\sum_{i=1}^{\infty}\rho(i) = \infty, \quad \sum_{i=1}^{\infty}\rho^2(i) < \infty$$

and

$$\lim_{i\to\infty}\rho(i) = 0$$

courtesy of [15]. To satisfy the constraints for ρ, then, we use

$$\rho(i) = 0.5\rho(i-1), \qquad i = 1, 2, 3, \ldots$$
$$\rho(0) = 0.5.$$

The approximation is completed when the partial derivatives are 0, or when

$$\mu_k(i+1) = \mu_k(i)$$
$$\omega_k(i+1) = \omega_k(i)$$
$$\delta_k(i+1) = \delta_k(i).$$

D. Step 4: Testing for Bimodality

To obtain reliable thresholds, only histograms which pass a bimodality test are used. Bimodality can be measured by the valley-to-peak ratio:

$$\delta = \frac{\text{minimum of } f() \text{ in } [\mu_1, \mu_2]}{\text{minimum of } f(\mu_1) \text{ and } f(\mu_2)}$$

where $f()$ is the Gaussian curve approximation whose coefficients were found in the previous step. The threshold value used for bimodality is $\delta < 0.8$.

E. Step 5: Region Thresholding

Those regions whose histograms passed the bimodality test of the previous stage are selected for thresholding. The threshold of each of those regions is computed according to the following quadratic formula derived from the method of maximum likelihood for the value of T which minimizes the probability of misclassification:

$$\left(\frac{1}{\sigma_1^2} - \frac{1}{\sigma_2^2}\right)T^2 + 2\left(\frac{\mu_2}{\sigma_2^2} - \frac{\mu_1}{\sigma_1^2}\right)T + \frac{\mu_1^2}{\sigma_1^2} - \frac{\mu_2^2}{\sigma_2^2} + 2\ln\frac{c_2}{c_1} = 0.$$

F. Step 6: Threshold Clustering

The calculated thresholds are separated into two groups (one group to represent the threshold point between Class 1 and Class 2, the other to represent the threshold point between Class 2 and Class 3). This is done by clustering the threshold points such that the variances within the two groups of thresholds which are formed by that clustering are minimized. We then have a group of thresholds which we say represent T_0, and another group to represent T_1.

G. Step 7: Interpolation of Region Thresholds

Regions with histograms not passing all bimodality tests have no thresholds at this point, and those that did pass the tests have only one. Two thresholds are needed for every region of the image. To fill in the missing thresholds, we interpolate the Class 1–Class 2 thresholds and the Class 2–Class 3 thresholds throughout the entire image.

Let $t_{m,n}$ be a threshold calculated for the region which is mth from the left and nth from the top of the image (if none, $t_{m,n} = 0$). The distance from that region is defined as square distance: the neighbors with distance 1 are the eight regions $(m+1, m)$, $(m+1, n-1)$, $(m, n-1)$, $(m-1, n-1)$, $(m-1, n)$, $(m-1, n+1)$, and $(m+1, n+1)$. The set of regions of distance one from m, n are denoted by $R(m, n, r)$. The weighting function used is a function of r:

$$w(r) = (1/\text{maximum radius allowed}) \times (\text{maximum radius allowed} - r).$$

Thus a region's own weight with respect to itself is 1, and the weight of neighboring regions decreases as their distance from that region increases. The number we use for the maximum radius allowed is the number of rows (or number of columns)-2.

Regardless of whether or not a region has been assigned a threshold, we look to the neighbors to increase the confidence that a proper threshold is being assigned to that region. The confidence is measure by the Q function [13]:

$$Q(m, n, r) = \sum_{(i,j)\in R(m,n,r)} w(r)u(t_{i,j})$$

where

$$u(t_{i,j}) = \begin{cases} 1 & \text{if } t_{i,j} > 0 \\ 0 & \text{if } t_{i,j} = 0 \end{cases}$$

$t_{i,j}$ = threshold value computed for region i, j.

When the total sum $\sum_{k=1}^{r} Q(m,n,k)$ exceeds a certain threshold Q_0, the interpolation terminates at neighbors of distance r. So when enough weighted neighboring regions have been found which have computed thresholds, the confidence of having a good threshold for that region is high enough to stop interpolation.

The threshold estimated for that region is then the weighted average of the thresholds of neighboring regions normalized by the confidence measure:

$$s_{m,n} = \frac{\sum_{k=1i}^{r} \sum_{i,j \in R(m,n,r)} w(k) t_{i,j}}{\sum_{k=1}^{r} Q(m,n,k)}.$$

We use a Q_0 of 1.25. This forces a smoothing operation on those regions which already have a threshold value assigned to them since a region's weight with respect to its own interpolation is 1.0.

We perform this procedure for both the T_0 and the T_1 values of every region so that each region of the image has two threshold points.

H. Step 8: Pointwise Interpolation

To ensure continuity in the boundary points on or near the border of two neighboring regions, pointwise bilinear interpolation is performed among the center points of the regions closest to that point.

The points at the corners and the edges of the image, however, are not in a square bounded by four region centers. Instead, every point of each corner gets the threshold values of the nearest region center, or the region located in that corner. Points in the top and bottom edges are assigned the thresholds of the point vertically nearest to them, while points along the side edges are assigned the thresholds of the point horizontally nearest to them. In this manner, every point in the image is assigned its own threshold values.

I. Step 9: The Trinary Decision

Based on the threshold values for each point previously computed in Step 9, each point in the image is thresholded to a value of 0, 128, or 255, corresponding to ice thicknesses of < 30 cm, 30–200 cm, and >200 cm, respectively:

$$\text{output}[i][j] = \begin{cases} 255 & \text{if} \quad \text{image}[i][j] \geq T_{p1}[i][j] \\ 128 & \text{if} \quad T_{p0}[i][j] \leq \text{image}[i][j] < T_{p1}[i][j] \\ 0 & \text{if} \quad \text{image}[i][j] < T_{p0}[i][j] \end{cases}.$$

This technique results in distinctions among three ice thickness classes: 0–30 cm, 30–200 cm, and >200 cm. It achieves these distinctions without being dependent upon predefined intensity thresholds which mandate the divisions among ice thickness classes.[1] Predefined values are often dependent upon location and season and can lead to errors in ice thickness classifications. Because the thresholds found by the dynamic local thresholding technique are computed from the data itself, each image is used to identify its own ice thickness classes.

[1] The current implementation of the methodology is dependent on a priori defined total number of ice classes, and current work is trying to address this issue.

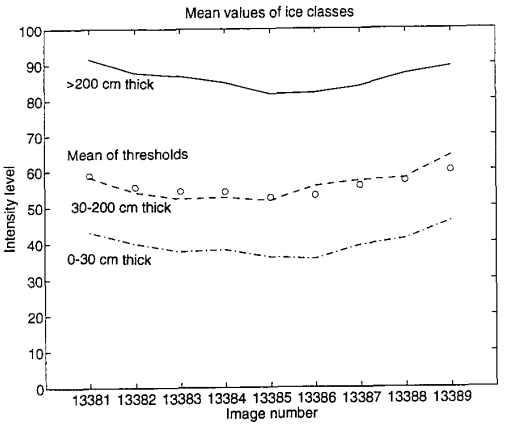

Fig. 1. Graph of average computed thresholds versus average gray level intensities of the ice thickness classes. Note that the thresholds average follows the trend of the average intensities.

As an illustration of this, consider Fig. 1. We conducted an experiment in which we analyzed the thresholding results of a series of images-an ERS-1 pass on Julian day 89 of 1992 which originated in the Beaufort Sea and terminated in the Arctic Basin. We found that the average of the thresholds selected by our technique was varying from image to image. We then extracted chunks of different ice thickness categories from those images using visual judgment and discovered the trend illustrated by Fig. 1. As can be seen in this figure, the average gray levels of the ice thickness classes themselves were fluctuating, resulting in the corresponding fluctuation in the thresholds selected. Because the technique adapts to the varying intensities of the ice classes, it is appropriate for sea ice classification and a good method for separating ice thickness classes.

IV. Feature Extraction

As stated previously, all floes and leads in the image must be individually defined-touching floes must be distinguished as two separate floes to give valid features to the expert systems stage. Thresholding techniques are certainly capable of indicating boundaries between regions composed of different ice thickness classes, but not boundaries between touching or overlapping regions of the same ice thickness class.

A technique was designed which combines multiple thresholdings, correlation, morphological cleaning, and structural growing. Multiple thresholdings and correlation are used to create two images. These images are then morphologically cleaned and recombined through a structural growing technique to produce a final image in which each feature is distinct and separate from all other features.

The two images generated are called the core and flesh images, in which the former produces separateness among floes and the latter produces fullness of features in terms of shape. Growing the core image within the boundary of the flesh image ensures both separateness and perseverance of shape in the final output.

Fig. 2. Dynamically thresholded ERS-1 SAR image used to illustrate the feature extraction technique.

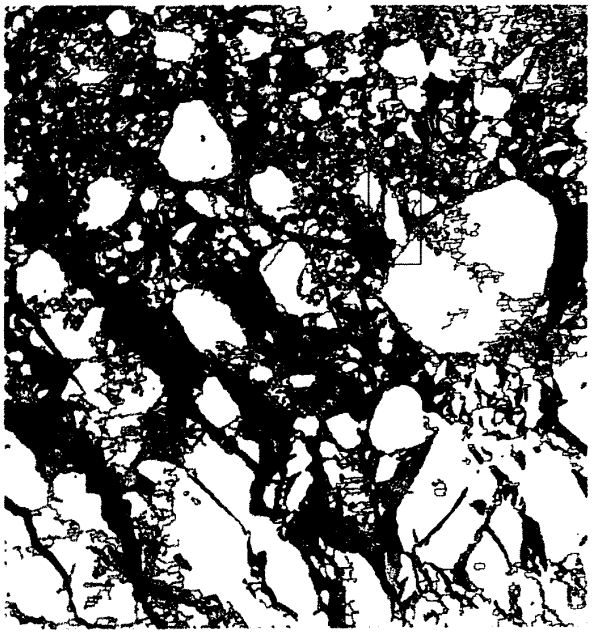

Fig. 3. Feature extracted version of Fig. 3. Note that the floes exhibit better separation from neighboring floes when compared to Fig. 3.

To generate the core and flesh images, we use multiple thresholdings and correlation. Correlation is a process that probabilistically labels a pixel into one of either object or non-object class based on the characteristics of its neighborhood exhibited at five different thresholded levels. The thresholds selected are based upon those supplied by the dynamic thresholding technique. Correlating the first three thresholded images yields the flesh image, while correlating all five images yields the core image. A sequence of morphological operators, dilation and erosion [16] are used to clean up both images. To attain the final image, we use a structural growing algorithm modified from a skeletonization algorithm [17]. This procedure grows a pixel in the core image from a non-object to an object pixel structurally such that an ice feature can regain its fullness in terms of shape without reconnecting to its adjacent neighbors [18].

To accommodate three-class images, the algorithm is executed twice on two different binary images. The first image consists of the lowest-intensity class and the union of the two other classes; the second image consists of the highest-intensity class and the union of the two other classes. Essentially, the algorithm is based on the following principles: assume three classes, c_1, c_2, c_3. The first step generates edges separating c_1 from $c_2 + c_3$; the second step separates $c_1 + c_2$ from c_3; as a result all three classes are then separated. Fig. 3 shows the results of applying the algorithm to a dynamically thresholded ERS-1 SAR image, shown in Fig. 2. To make the small details more apparent, we have selected a piece of the ice for enlargement, shown as a red rectangle in each of the two figures. These results can be seen in Fig. 4.

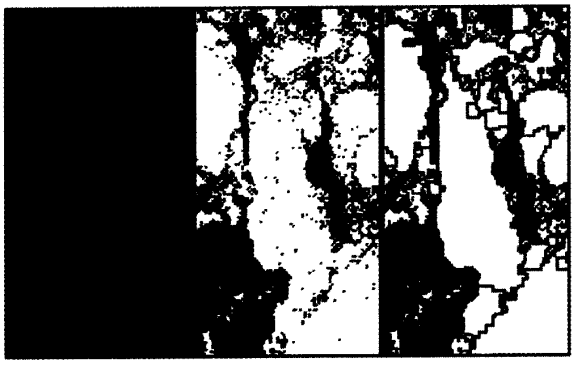

(a) (b) (c)

Fig. 4. Enlargement of highlighted areas in Figs. 3 and 4, illustrating the feature extraction technique. (a) Raw data corresponding to highlighted areas in Figs. 3 and 4. (b) Enlargement of highlighted area of Fig. 3. Notice the absence of distinct floe boundaries. (c) Enlargement of highlighted area of Fig. 4. The boundaries created by the feature extraction technique are shown in red.

Fig. 4(a) is the original data corresponding to the enlarged area. We can visually distinguish the separate floes within the area of ice. In the enlargement of Fig. 4(b), which is a locally thresholded version of 4(a), we can see *hints* of boundaries among the ice floes, but no definite separations. In image 4(c), however, the boundaries created by the feature extraction program, shown in red, combine with the natural boundaries to make the distinctions between the floes quite clear. Without this extraction technique, the small collection of floes in Fig. 4 would be seen as one large blob and would not reflect the data that was truly there. Using the feature extraction program, we can obtain size and shape characteristics for the features which reflect the content of the original data.

TABLE I
FEATURES USED IN THE EXPERT SYSTEMS AND THEIR MEANINGS

Characteristic	Literal Measure
perimeter	Used in assessing the size and elongation of a feature
area	Provides a size estimation for a feature
wiggliness Sum of absolute values of difference between each successive link in chain code	Measures the visually perceived "smoothness" of a feature's edge or boundary
circularity Standard deviation of distance between points on perimeter and centroid of feature	Measures the visually perceived "roundness" of a feature
elongatedness Length-to-width ratio of bounding rectangle multiplied by a compactness measure	Estimates the length to width ratio of a feature (how long and narrow it is)
adjacent-to	Indicates what other features a given feature is sharing a boundary with, or "touching"
enclosed-by	Indicates that a given feature is completely surrounded by another feature

V. FEATURE CHARACTERISTIC MEASUREMENT

The extraction of features and their characteristics is necessary for the analysis of the image through the use of expert systems. Any contiguous set of pixels having identical thresholded values (0, 128, or 255) is called a feature. By grouping adjacent pixels with identical values, features within the image can be identified and given an initial classification according to the classification of the pixels of which they consist; i.e., features consisting of 0-value pixels are called <30 cm, those consisting of 128-value pixels are called 30–200 cm, and those consisting of 255-value pixels are given classifications of >200 cm ice. These features can then be analyzed with respect to their geometric characteristics and their positional relations to other features in the image (A is enclosed by B, B is adjacent to C, etc.).

The geometric characteristics of each feature are very important for future analysis by expert systems; these include measures related to size, shape, and edge smoothness (area, circularity, elongatedness, and wiggliness). These geometric characteristics were selected to satisfy the rules of the expert system stage. For example, old ice (>200 cm thick) is never extremely elongated. Therefore, if a feature is found which has an initial classification of >200 cm and which is very elongated, then the feature is possibly reclassified as first-year ice or as windy open water. It is rules such as this which mandate which geometric characteristics are extracted from the features.

Each feature is defined symbolically through both its geometric characteristics and its positional relationships with other features in the image so that the expert system stage may perform the best analysis possible. A table describing the possible characteristics of a feature is given below: These characteristics were selected to satisfy the requirements of the ice growth and behavior models implemented in the expert systems stage.[2]

[2]In this paper we concentrate on dynamic thresholding and its integration with the expert systems to produce a comprehensive system. In the text, our discussion of the expert systems and the feature and feature characteristics extractions will be limited, and interested readers are referred to [19].

VI. GEOPHYSICAL KNOWLEDGE APPLICATION

We coded qualitative models concerning the growth and behavior of sea ice and the historical and geographical information into a rule-based expert system using CLIPS [20]. Rules result in changes to the ice fact base when the left-hand side of a rule matches facts in the fact base. The facts concern the classifications of, the geometric characteristics of, and the positional relationships between features in a SAR image, in addition to geographic location and time of year. The final classifications of all features are mandated by the final state of the world as represented in the fact base.

A. Growth and Behavior Models

Experts in the field of sea ice classification can correctly classify many ice features which cannot be identified successfully through automated methods. Rules concerning sea ice growth and behavior were defined and are applied by the SAR classification expert system. For each rule shown below, we show the text definition followed by the expert system interpretation. Many of these rules (only a couple of which are shown here) provide for the identification of special geophysical features in the ice such as ridges, meltponds, leads, and refrozen leads. See [19] for additional rules and details.

1) Meltpond: Small open water patches located in the midst of ice which is greater than 200 cm thick are most likely meltponds, often formed in the warm season. Meltponds are pools of melted ice on the top of the floe. They are not equivalent to open water, which would indicate a hole in the floe which continued to the water below and which represents a heat source. A break in the floe would not be a hole, anyway; it would be an elongated fracture in the ice. By looking for patches of water in a >200 cm thick ice floe which are not elongated, we can identify meltponds. Upon identification, the classification of a meltpond (open water) is altered to ice with a thickness of >200 cm. In addition, it is identified as

a geophysical feature. The actual rule is equivalent to the following:

```
if      (class feature1 <30 cm)
  and   (shape feature1 circular)
  and   (size feature1 very-small)
  and   (feature1 enclosed-by feature2)
  and   (class feature2 >200 cm)
  and   (or (size feature2 large) (size feature2 very-large))
then
        (retract (class feature1 <30 cm))
  and   (assert (class feature1 >200 cm))
  and   (assert (type feature1 MELTPOND))
```

Without this rule, areas of meltponding could be mistaken as open water, resulting in incorrect approximations of heat flux: the heat flux of thick ice is approximately 7 W/m^2, compared to 200 W/m^2 for open water. During the melt season, this could result in large errors in the estimated heat flux.

2) Wind-Roughened Open Water: Wind-roughened open water is often misclassified as thick ice because a slight wind as little as 5 mph causes a dramatic increase in the backscatter of the open water. If a feature is extremely elongated and has been initially classified as >200 cm thick ice, then we assume that it is, in fact, a patch of wind-roughened open water which has been misclassified. This information also indicates that there cannot be any open water in the image which is *not* wind-roughened open water, thus altering the classifications of any features initially classified as open water, or <30 cm thick. We also flag the occurrence as the geophysical phenomena *wind-roughened open water*, denoted by WOW. The corresponding rule is as follows:

```
if      (class feature1 >200 cm)
  and   (shape feature1 elongated)
  and   (edge feature1 not-wiggly)
  and   (or (size feature1 very-small) (size feature1 small)
            (size feature1 medium))
then
        (retract (class feature1 >200 cm))
  and   (assert (class feature1 < 30cm))
  and   (assert (type feature1 WOW))
  and   (assert (exist WOW))
```

B. Historical and Geographical Information

We used ice concentration maps generated by the Joint Ice Center in Washington, DC [21] to create ice concentration guidelines for every region of the northern oceans for each month of the year. An example rule would be as follows:

```
if      (region BeringSea)
  and   (time-of-year June)
  and   (or (<30 cm >10) (>200 cm >10%))
then
        (assert (FLAG "<30 cm ice or >200 cm ice
                       present in Bering Sea during June"))
```

which simply states that if the image is taken from the Bering Sea during June, there should be no more than 10% coverage of 0–30 cm thick ice, and no more than 10% coverage of >200 cm thick ice.

Rules of this type cause no changes in classification. Instead, they detect the possible presence of error in the classifications. We are currently modifying the rules to cause changes in the level of confidence to which we believe the classification of any given feature.

VII. Testing and Results

Various images of sea ice were processed by the system in order to test its appropriateness for sea ice classification. We will present results of both the local thresholding technique alone, and the results of the entire system as a whole. Our intent is to show that the local thresholding technique is a correct first step for the system, and to exhibit the merit of using geophysical information and knowledge in sea ice classification.

A. Data Set

We tested on approximately 90 ERS-1 sea ice images. We selected images which were dynamic in content; i.e., containing floes and leads and two or more ice thickness groups. All images were 1024 × 1024 pixels in size, stored as one byte per pixel. The system requires approximately five minutes to fully classify an image on a DECstation 5000/240.

B. Results

Our goal in classification was to distinguish among <30 cm thick ice, 30–200 cm, and >200 cm ice. In all of the figures used to illustrate our results, black corresponds to a classification of 0–30 cm thick ice, while gray corresponds to 30–200 cm thick ice, and white corresponds to >200 cm thick ice. We find that the dynamic thresholding technique offers good separation of ice classes. Inherent problems caused by the SAR portrayal of the ice under varying environmental conditions are remedied to a large extent by the expert systems analysis. Of course, as in most sea ice classification research, where extensive *in situ* verifications are difficult or impossible, our evaluation of the results of our algorithms are necessarily qualitative, and based on visual inspections of the resulting classification maps.

1) Dynamic Thresholding: We have here some examples to illustrate the ability of the technique to separate an image into classes. Fig. 5 is an ERS-1 image taken on Julian day 80 of 1992 in the Beaufort Sea at 72.8° N, −143.8° E.[3] Fig. 7 is the result of dynamic thresholding on that image. Compared to a global thresholding technique (see Fig. 6), the segmentation better reflects the separation between ice types which we see when we look at the original image (Fig. 5).

Fig. 8 is an example of an ERS-1 SAR image taken on Julian day 253 of 1992 at location 73.6° N, −162.9° E. Notice the backscatter reversal in the image: the thinner ice types are bright and the thicker types are dark. The globally thresholded image is shown in Fig. 9, while the dynamically thresholded version is shown in Fig. 10. Notice the lower right-hand corner of the image (Fig. 8). The ice

[3] This was the approximate LEADEX area [22].

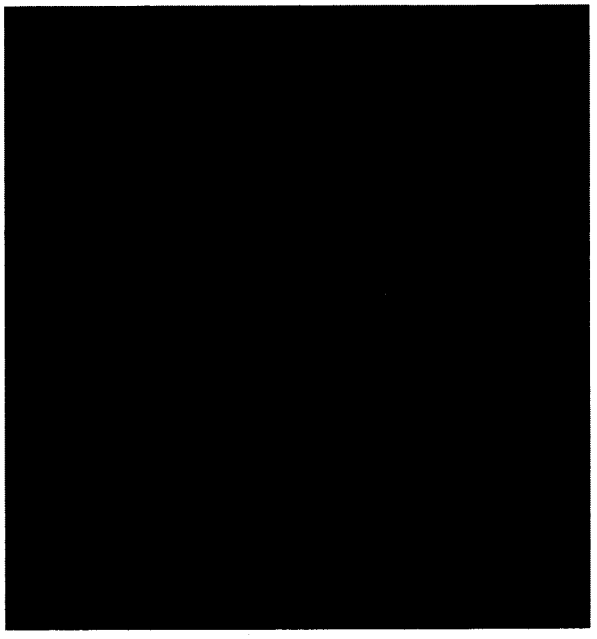

Fig. 5. ERS-1 image from the LEADEX area used to illustrate the dynamic local thresholding technique. In the darker areas of the image, there are visible ridges or cracks within the ice. Copyright ESA.

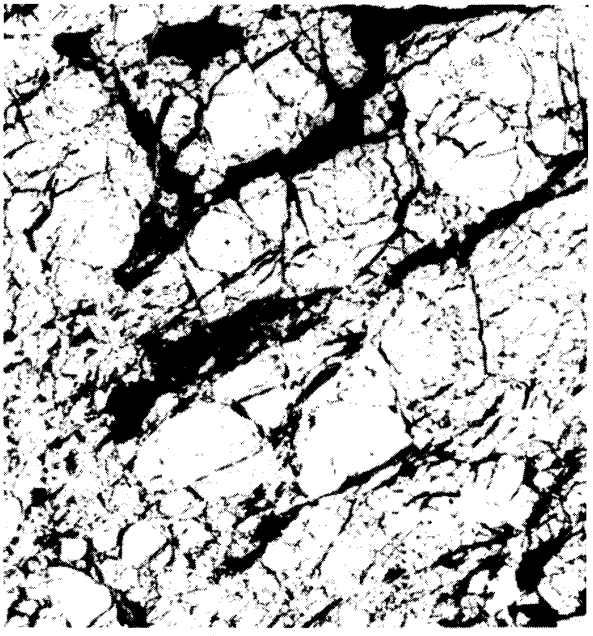

Fig. 6. Result of global thresholding on Fig. 5. Note the absence of the ridges and cracks that are visible in Fig. 5.

floes are absorbed into the background matrix when globally thresholded. Fig. 10, however, retains distinction between the floes and the background matrix of ice. Again, by visual judgment, the local thresholding technique preserves more contrast throughout the image and achieves a better class separation.

Fig. 7. Result of dynamic local thresholding on Fig. 5. Note that more image contrast is preserved when compared to the globally thresholded result (Fig. 6). Note especially the gray cracks within the black features which are now apparent in the upper portion of the image.

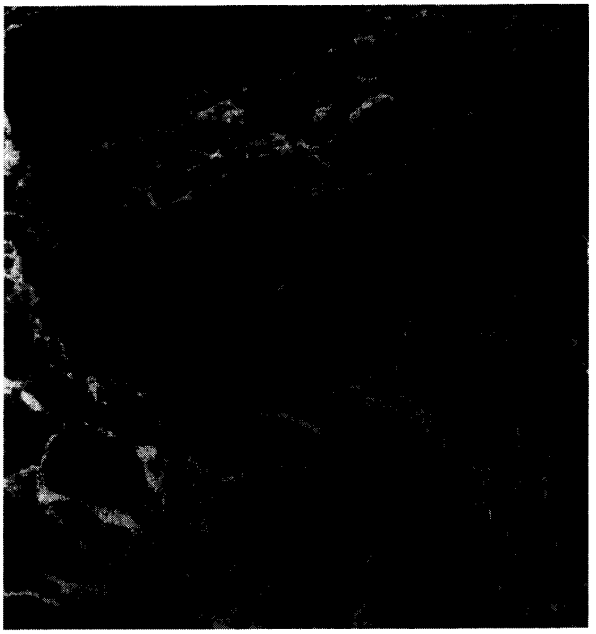

Fig. 8. ERS-1 image from summertime used to illustrate the dynamic local thresholding technique. In the lower right corner of the image, there is a conglomeration of small floes frozen together. The background ice into which these are frozen has a backscatter which is different from the adjacent large ice floes above and to the left. Copyright ESA.

2) Expert Systems: Some of the biggest difficulties in the classification of ERS-1 SAR imagery stem from the geophysical properties of the ice itself: melting effects and wind

Fig. 9. Result of global thresholding on Fig. 8. The conglomeration of small floes in the lower right corner has become invisible (see Fig. 8). There is no longer a distinction between the background ice of the conglomeration and the adjacent ice floes.

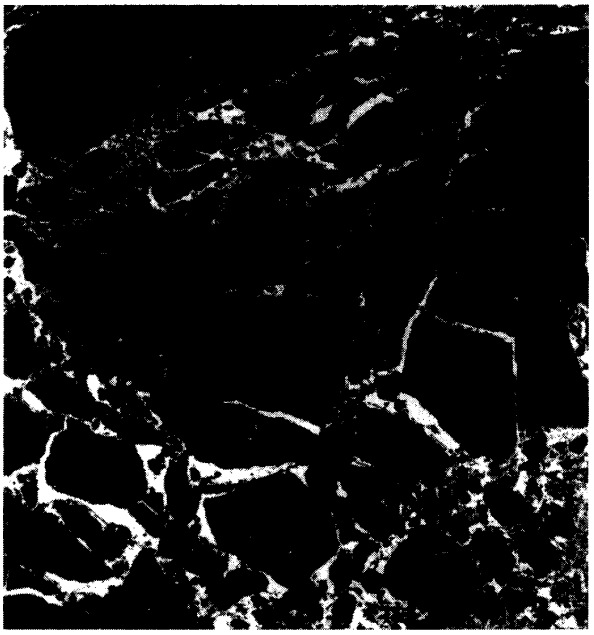

Fig. 10. Result of dynamic local thresholding on Fig. 8. Note the preservation of more of the contrasts of the original image when compared to the globally thresholded result (Fig. 9). The conglomeration of small ice floes at the lower right corner of the image is much more apparent. The background ice of the conglomeration is now distinguishable from the surrounding large ice floes, as it was in the original image (Fig. 8).

effects cause the ice thickness classes to exhibit backscatter characteristics which are different from the norm.

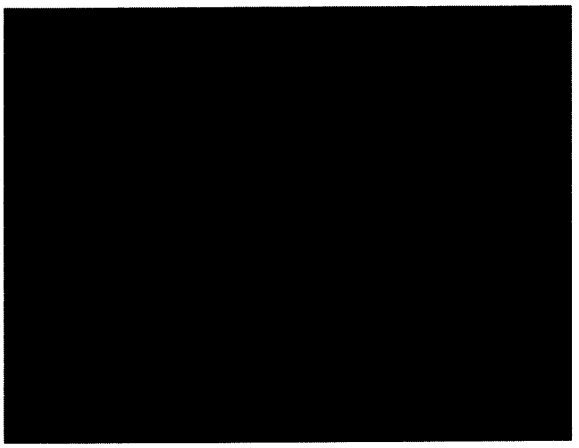

Fig. 11. Part of an ERS-1 image containing wind-roughened open water and used to illustrate the performance of the expert systems. The open water is in a matrix of >200 cm thick ice, with some 30–200 cm ice present also. Copyright ESA.

Fig. 12. Result of dynamic local thresholding on Fig. 11. Black represents 0–30 cm thick ice, gray represents 30–200 cm thick ice, and white represents >200 cm thick ice. The wind-roughened open water has been classified as >200 cm thick ice.

Consider Fig. 11. In this image, we have some wind-roughened open water and first-year ice (30–200 cm thick) in a matrix of multi year ice >200 cm thick). Because of the wind factor, the open water now has an intensity level in the acceptable >200 cm thick ice range. After the local thresholding technique separates the classes, the brightest class is labeled >200 cm thick. This leads to the incorrect labeling of the wind-roughened open water as ice (see Fig. 12). The extracted features and their characteristics are fed to the expert systems. Because the features initially classified as >200 cm thick ice are elongated and have a straight edge indicative of an open water feature, they are reclassified as <30 cm thick. In turn, the existence of wind-roughened open water forces changes in the remaining features (since there can now be *no* open water unless it is *wind-roughened* open water), and the resulting classification can be seen in Fig. 13. The wind-roughened open water is now correctly classified as <30 cm.

Fig. 13. Result of expert systems on the locally thresholded image (Fig. 12). The wind-roughened open water has been identified and reclassified as <30 cm thick ice. This discovery redefined the classifications of the other features in the image: because wind-roughened open water was found, the features originally classified as <30 cm thick were reclassified as 30–200 cm thick, and those originally classified as 30–200 cm thick were reclassified as >200 cm thick (black = 0–30 cm, gray = 30–200 cm, white =>200 cm).

VIII. Conclusion

We have presented results showing the merit of the local thresholding technique. It achieves a good separation among ice thickness classes. Where global thresholding techniques often lose the contrast of the original image, the local dynamic thresholding procedure preserves it. This technique responds to relative intensity levels within the image and adapts well to changes in the signatures of the ice thickness categories. The expert systems are often capable of achieving the correct reclassifications of features which were initially misclassified as a result of geophysical changes which alter the backscatters of the ice classes.

In conclusion, the local thresholding technique used in the system presented is appropriate for ice classification because it does not require gray level consistency across images and can adapt to the inherent inconsistencies in the backscatters of the different sea ice thickness categories. Using geophysical classification knowledge (ice growth and behavior, geographical, historical) to supplement the original classification, the proper labelings for the ice thickness classes in the image can be achieved.

Acknowledgment

The authors would like to thank everyone at the Naval Research Laboratory at the John C. Stennis Space Center in Mississippi, particularly Florence Fetterer and Denise Gineris for their assistance in data retrieval and for sharing their knowledge concerning sea ice imagery.

References

[1] A. Rosenfeld and L. S. Davis, "Iterative histogram modification," *IEEE Trans. Syst. Man Cybernet.*, vol. SMC-8, pp. 300–302, Apr. 1978.

[2] K. A. Narayanan and A. Rosenfeld, "Image smoothing by local use of global information," *IEEE Trans. Syst. Man Cybernet.*, vol. SMC-11, pp. 826–831, Dec. 1981.

[3] E. Alparslan and F. Ince, "Image enhancement by local histogram stretching," *IEEE Trans. Syst. Man Cybernet.*, vol. SMC-11, pp. 376–385, May 1981.

[4] N. Ahuja and A. Rosenfeld, "A note on the use of second-order gray-level statistics for threshold selection," *IEEE Trans. Syst. Man Cybernet.*, vol. SMC-8, pp. 895–898, Dec. 1978.

[5] J. S. Weszka and A. Rosenfeld, "Histogram modification for threshold selection," *IEEE Trans. Syst. Man Cybernet.*, vol. SMC-9, pp. 38–52, Jan. 1979.

[6] B. Holt, R. Kwok, and E. Rignot, "Ice classification algorithm development and verification for the alaska sar facility using aircraft imagery," in *Int. Geosci. Remote Sensing Symp. (IGARSS '89)*, 1989, pp. 751–754.

[7] T. Tjahjadi and R. Henson, "A knowledge-based system for image understanding," in *IEE 3rd Int. Conf. Image Processing and its Appl.*, 1989, pp. 88–92.

[8] T. Matsuyama, "Knowledge-based aerial image understanding systems and expert systems for image processing," *IEEE Trans. Geosci. Remote Sensing*, vol. GE-25, pp. 305–316, May 1978.

[9] M. D. Levine and A. M. Nazif, "Rule-based image segmentation: A dynamic control strategy approach," *Computer Vision, Graphics, and Image Processing*, vol. 32, no. 1, pp. 104–126, Oct. 1985.

[10] S. W. Wharton, "Spectral-knowledge-based approach for urban land-cover discrimination," *IEEE Trans. Geosci. Remote Sensing*, vol. GE-25, pp. 273–282, Mar. 1987.

[11] J. G. McAvoy and E. M. Krakowski, "A knowledge based system for the interpretation of SAR images of sea ice," in *Int. Geosci. Remote Sensing Symp. (IGARSS '89)*, 1989, pp. 844–847.

[12] C. Tsatsoulis, "Expert systems in remote sensing applications," IEEE Geoscience and Remote Sensing Society *Newslett.*, pp. 7–15, June 1993.

[13] C. K. Chow and T. Kaneko, "Automatic boundary detection of the left ventricle from cineangiograms," *Computers and Biomed. Res.*, vol. 5, pp. 388–410, 1972.

[14] T. Y. Young and G. Coraluppi, "Stochastic estimation of a mixture of normal density functions using an information criterion," *IEEE Trans. Info. Theory*, vol. IT-16, pp. 258–263, May 1970.

[15] R. L. Kashyap and C. C. Blaydon, "Estimation of Probability Density and Distribution Functions," *IEEE Trans. Info. Theory*, vol. IT-14, pp. 549–556, July 1968.

[16] M. Ejiri, T. Uno, M. Mese, and S. Ikeda, "A process for detecting defects in complicated patterns," *Computer Graphics and Image Processing*, vol. 2, pp. 326–339, 1973.

[17] T. Y. Zhang and C. Y. Suen, "A fast parallel algorithm for thinning digital patterns," *Commun. ACM*, vol. 27, pp. 236–239, 1984.

[18] L. K. Soh and C. Tsatsoulis, "A feature extraction technique for synthetic aperture radar (SAR) sea ice imagery," in *Int. Geosci. Remote Sensing Symp. (IGARSS'93)*, 1993, pp. 632–634.

[19] D. Haverkamp, C. Tsatsoulis, and S. Gogineni, "The combination of algorithmic and heuristic methods for the classification of sea ice imagery," *Remote Sensing Rev.*, vol. 9, 135–159, 1994.

[20] NASA, *CLIPS User's Guide*, Lyndon B. Johnson Space Center, Mission Support Directorate, 1986.

[21] *Eastern–Western Arctic Ice Analysis*, 1992, prepared by the Naval Polar Oceanography Center, Suitland, MD, under the authority of the Commander, Naval Oceanography Command, Stennis Space Center, MS 39529-5004.

[22] R. Schuchman and R. Onstott, "Characterization of ERS-1 SAR snow and sea ice signatures during LEADEX," ERIM Interim Rep., 1992.

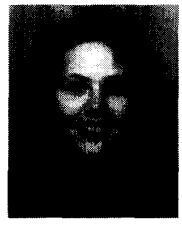

Donna Haverkamp (S'94), received the B.S. degree in computer engineering and the M.S degree in electrical engineering at the University of Kansas, Lawrence, in 1990 and 1992, respectively. She is pursuing the Ph.D. degree at the same university.

Her research interests include image processing and artificial intelligence. She is currently a NASA Clobal Change Research Fellow.

Ms. Haverkamp is a member of Tau Beta Pi, Eta Kappa Nu, ACM, and AAAI.

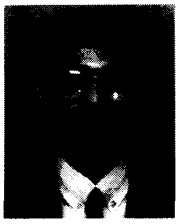

Leen Kiat Soh (S'94) was born in Johor, Malaysia. He received the B.S. and M.S. degrees in electrical engineering from the University of Kansas, Lawrence, in 1991, and 1993, respectively. He is pursuing the Ph.D degree at the same university.

His research interests are in the areas of image processing, computer vision, expert systems, and case-based reasoning.

Mr. Soh is a member of Phi Kappa Phi, Tau Beta Pi, Eta Kappa Nu, and Phi Beta Delta

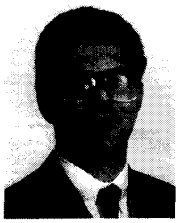

Costas Tsatsoulis (M'88) received the Ph.D. in electrical engineering from Purdue University, East Lafayette, IN.

He is currently an Assoicate Professor of Electrical Engineering and Computer Science at the University of Kansas, Lawrence. His research interests are in the application of artificial intellignece to imagery classification, information retrieval, and design. He is also working on theoretical aspects of distributed AI and case-based reasoning. He has published more than 50 papers in the area of AI, and has lead many research projects.

Dr. Tsatsoulis is an Associate Editor of *IEEE Expert*, and Area Editor of *The AI Magazine*, and a member of ACM and AAAI.